JOURNAL OF Applied Polymer SCIENCE

A Novel Route for the Synthesis of Poly(2-hydroxyethyl methacrylate) Grafted TiO_2 Nanoparticles via Surface Thiol-Lactam Initiated Radical Polymerization

Long Giang Bach,[1] Md. Rafiqul Islam,[1] Sung Yong Seo,[2] Kwon Taek Lim[1]
[1]Department of Imaging System Engineering, Pukyong National University, Busan 608-737, Korea
[2]Department of Chemistry, Pukyong National University, Busan 608-737, Korea

Correspondence to: K. T. Lim (E-mail: ktlim@pknu.ac.kr)

ABSTRACT: Hybrid nanocomposites of poly(2-hydroxyethyl methacrylate) (PHEMA) and TiO_2 nanoparticles were synthesized via surface thiol-lactam initiated radical polymerization by following the grafting from strategy. Initially, TiO_2 nanoparticles were modified by 3-mercaptopropyl trimethoxysilane to prepare thiol functionalized TiO_2 nanoparticles (TiO_2—SH). Subsequently, surface initiated polymerization of 2-hydroxyethyl methacrylate was conducted by using TiO_2—SH and butyrolactam as an initiating system. The anchoring of PHEMA onto the surface of TiO_2 nanoparticles was investigated by FTIR, ^{1}H-NMR, XPS, TGA, and XRD analyses. The experimental results indicated a strong interaction between PHEMA and TiO_2 nanoparticles owing to covalent bonding. The TEM and SEM images of PHEMA-*g*-TiO_2 showed that the agglomeration propensity of TiO_2 nanoparticles was significantly reduced upon the PHEMA functionalization. The molecular weight and polydispersity index of the cleaved PHEMA from the surface of TiO_2 nanocomposites were estimated by GPC analysis. An improved thermal property of the nanocomposites was observed from TGA analysis. PHEMA-*g*-TiO_2 nanocomposites were found to be highly dispersible in organic solvents. © 2012 Wiley Periodicals, Inc. J. Appl. Polym. Sci. 000: 000–000, 2012

KEYWORDS: TiO_2 nanoparticles; poly(2-hydroxyethyl methacrylate); hybrid nanocomposites; polymer brush; surface initiated polymerization; grafting from

Received 30 August 2011; accepted 12 April 2012; published online
DOI: 10.1002/app.37879

INTRODUCTION

Over the past few decades, development of novel materials with desired properties has attracted tremendous attention in material sciences due to their versatile applications. More specifically, nanocomposites comprising biocompatible polymer matrices and inorganic nanoparticle fillers have become a dependable source of composite biomaterials for tissue engineering scaffolds and biomedical implants and devices.[1–5] It is well known that incorporation of ceramic nanoparticles, such as alumina or titania to polymer matrices significantly alters their physical, mechanical and biological properties.[6–8] Recently, TiO_2 has drawn considerable interest because of their potential applications as chemical sensors, biomedical materials, and a glass coating material for antifogging and self-cleaning. A few studies have demonstrated that TiO_2 could act as a bioactive material by exhibiting strong interfacial bonding to living tissue.[9–12]

In some biomedical applications, it is desirable to functionalize TiO_2 with polymer shells bearing specific functional groups capable of conjugation or immobilization of foreign biological molecules. Poly(2-hydroxyethyl methacrylate) (PHEMA) is one of the most widely used hydrogels for various biomedical applications such as drug delivery systems, tissue engineering, and contact lenses because of its biocompatibility.[13–17] High density of hydroxyl groups within PHEMA hydrogels provides a hydrophilic surface that exhibits low interfacial free energy with most body fluids, resulting in minimal adhesion of proteins and cells to their surfaces. The combination of excellent biocompatible properties of PHEMA and the beneficial characteristics of TiO_2 produced a promising composite biomaterial for tissue engineering scaffolds and biomedical implants and devices.[18–22]

Numerous strategies for improving the interfacial bonding and overall performance of polymer nanocomposites have been reported.[23–25] The grafting from method is currently put in practice to carry out the direct polymerization on solid surfaces. The advantage of grafting from strategy over other surface modification methods is their ability to precisely control the

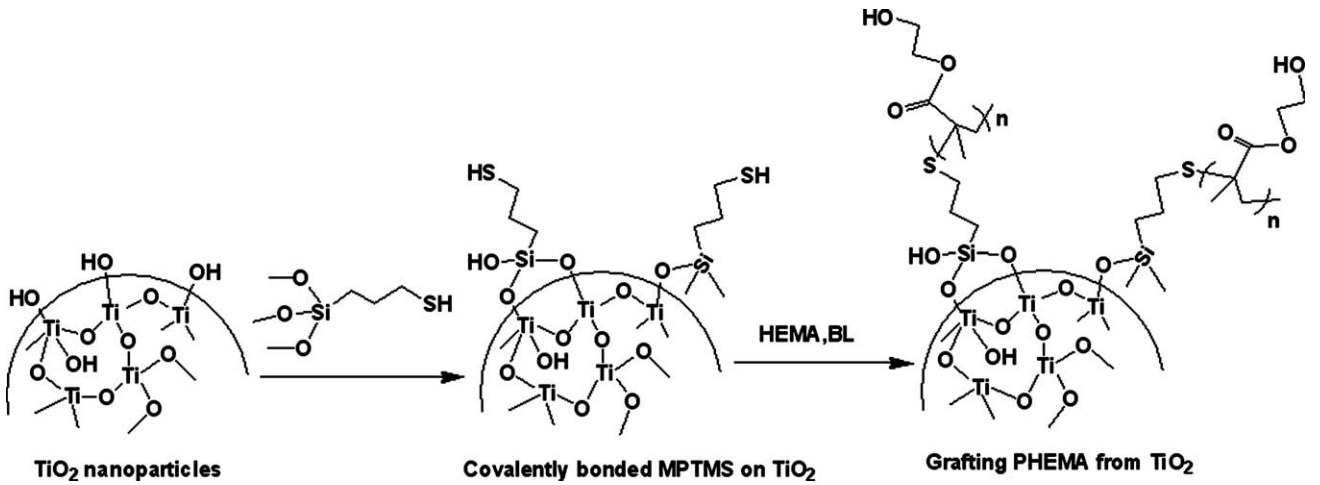

Scheme 1. The synthetic route for the preparation of PHEMA grafted TiO_2 nanocomposites.

molecular weight and grafting thickness coupled with a high degree of synthetic flexibility towards the introduction of a variety of functional groups.[26–30] Recently, a few reports have been published on the grafting of PHEMA or its copolymer onto TiO_2 surfaces including controlled radical polymerization.[31–33] Development of a facile and more effective strategy for the surface grafting of TiO_2 nanoparticles by biocompatible PHEMA is required to fabricate well dispersed nanocomposites. We have recently reported a simple grafting from protocol for the synthesis of inorganic/polymer nanocomposites materials via surface thiol-lactam initiated radical polymerization (TLIRP) technique using surface bonded thiol functionalized nanoparticles and butyrolactam (BL).[34–36] Because of its tolerance to a wide range of reaction conditions, the TLIRP protocol could be thought as a simple and efficient operational method for the surface modification of nanoparticles.

In this study, chemically anchored PHEMA with TiO_2 nanoparticles was realized by using the facile TLIRP technique using the grafting from strategy. TiO_2 nanoparticles were functionalized by thiol groups and the subsequent grafting polymerization of HEMA from the TiO_2—SH surface was accomplished in the presence of BL. The surface composition, morphology and properties of the synthesized nanocomposites were investigated by respective spectroscopic and physical analyses.

EXPERIMENTAL

Materials

3-mercaptopropyl-trimethoxysilane (MPTMS), BL, TiO_2 nanoparticles (anatase), methanol, and toluene were purchased from Aldrich and used as received. HEMA was passed through a short column of basic alumina to remove inhibitors. Tetrahydrofuran (THF) was dried over CaH_2 and distilled prior to use.

Preparation of Thiol Functional TiO_2 Nanoparticles (TiO_2—SH)

The grafting of MPTMS on the surface of TiO_2 nanoparticles was carried out according to the reported procedure.[34] After dispersing 10 g of TiO_2 nanoparticles in 200 mL of toluene, an excess amount of MPTMS was added and the resulting solution was stirred for 24 h under argon atmosphere. Modified TiO_2 nanoparticles were isolated by centrifugation and washed repeatedly with toluene. Finally, it was dried at 40°C under vacuum for 24 h.

Synthesis of PHEMA Grafted TiO_2 Nanoparticles (PHEMA-*g*-TiO_2)

A typical procedure for the synthesis of PHEMA-*g*-TiO_2 nanocomposites by TLIRP is as follows: 1 g of HEMA, 0.2 g of TiO_2-SH, 0.4 g of BL, 3 mL of THF and a Teflon-coated stir bar were placed in a 25 mL round flask equipped with a reflux condenser. The flask was purged with nitrogen, heated to 80°C and kept stirring. By the end of the reaction, the viscosity of the reaction mixture increased dramatically. After the required time (8 h), the flask was cooled to room temperature and the reaction mixture was precipitated in a large excess of diethyl ether, and washed three times with THF. Finally, PHEMA-*g*-TiO_2 nanocomposites were dried in a vacuum oven at 40°C for overnight. A synthetic route for the preparation of PHEMA-*g*-TiO_2 is shown in Scheme 1.

Cleavage of the Grafted PHEMA from PHEMA-*g*-TiO_2 Nanocomposites

To determine the number-averaged molecular weight (M_n) and polydispersity index (PDI = M_w/M_n) of the grafted PHEMA, the PHEMA chains were cleaved from the PHEMA-*g*-TiO_2 nanocomposites using the following method. One hundred milligram of the PHEMA-*g*-TiO_2 nanocomposites were dissolved in the mixture of 1 mL of HCl (2 *M*) and 10 mL of *N*, *N*-dimethylformamide (DMF). The solution was allowed to stir at 80°C for 24 h. The cleaved PHEMA in the organic layer was precipitated in diethyl ether. The product was dried in vacuum at 40°C for 24 h.

Characterization and Measurements

The surface chemical bonding of TiO_2—SH and PHEMA-*g*-TiO_2 were investigated by Fourier transformed infrared spectrophotometry (FTIR) using a BOMEM Hartman & Braun FTIR Spectrometer in the frequency range of 4000–400 cm^{-1}. Surface composition was studied using X-ray photoelectron spectroscopy (XPS) (Thermo VG Multilab 2000) in ultra high vacuum with Al Kα radiation. The elemental analysis was carried out by

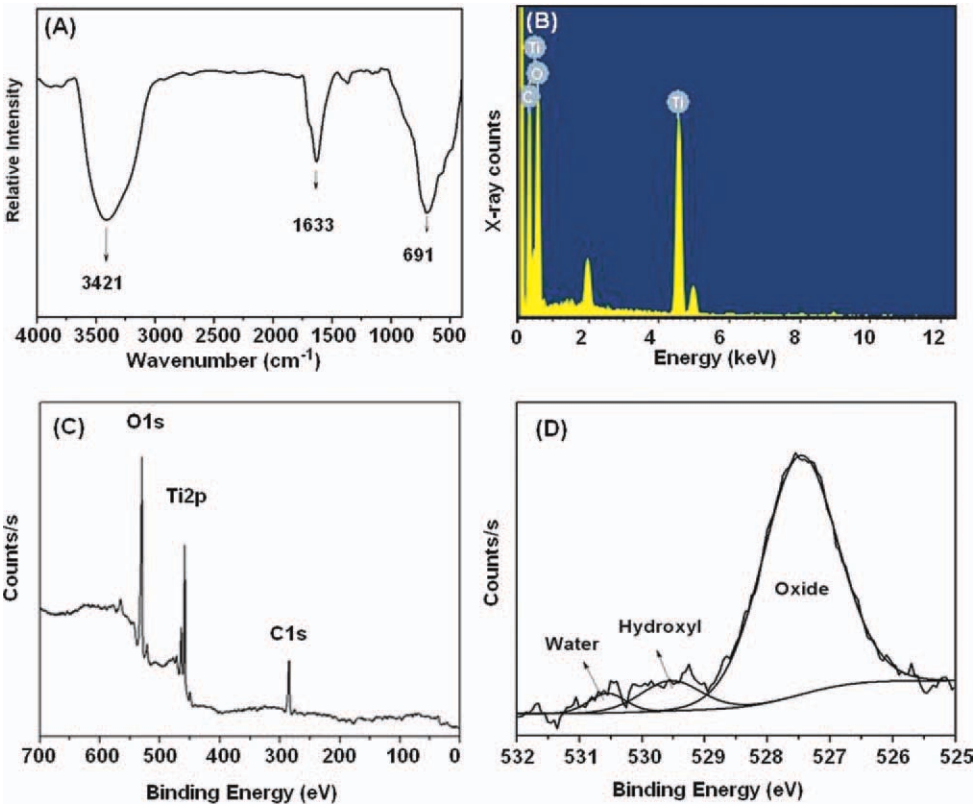

Figure 1. (A) FTIR spectrum, (B) EDX spectrum, (C) wide-scan spectrum, and (D) O1s core-level signals of TiO_2 nanoparticles. [Color figure can be viewed in the online issue, which is available at wileyonlinelibrary.com.]

using field emission scanning electron microscopy (FE-SEM) equipped with an energy dispersive X-ray (EDX) spectrometer (Hitachi JEOL- JSM-6700F system, Japan). Transmission electron microscopy (TEM) images were recorded using Joel JEM 2010 instrument (Japan) with an accelerating voltage of 200 kV. The hydrodynamic size of the PHEMA-*g*-TiO_2 nanocomposites was determined by dynamic light scattering (DLS) using a Brookhaven BI-200SM light scattering system (Brookhaven Instruments) at a measurement angle of 90°. Thermogravimetric analysis (TGA) was conducted with Perkin–Elmer Pyris 1 analyzer. Before the test, all the samples were carefully grinded into fine powder. The samples were scanned within the temperature range of 50–800°C at a heating rate of 10°C min^{-1} under the continuous nitrogen flow. The crystallographic state of PHEMA-*g*-TiO_2 was determined by a Philips X'pert-MPD system diffractometer (The Netherlands) with Cu Kα radiation. The ^{1}H-NMR spectrum of cleaved PHEMA was recorded using a JNM-ECP 400 (JEOL) spectrophotometer in CD_3OD. Gel permeation chromatography (GPC) analyses were carried out on an Agilent 1200 series equipped with PLgel 5 μm MIXED-C columns, with the DMF solvent at 30°C. The solution flow rate was 1 mL/min. Calibration was carried out using PMMA standards.

RESULTS AND DISCUSSION

The surface properties of TiO_2 nanoparticles were investigated using FTIR, EDX, and XPS. The characteristic strong absorption bands at 3421 and 1633 cm^{-1} were observed in the pristine TiO_2 nanoparticles due to the —OH stretching vibrations and H—O—H bending vibrations, respectively [Figure 1(A)]. The absorption bands between 500 and 800 cm^{-1} are assigned to the vibrations of Ti—O and Ti—O—Ti framework bonds.[27] The EDX and XPS analyses suggested the presence of Ti and O elements in TiO_2 nanoparticles as shown in Figure 1(B, C). Figure 1(D) shows high-resolution oxygen (O 1s) spectra for TiO_2 nanoparticles. These spectra show at least three resolved peaks at 527.6, 529.5, and 530.7 eV. The most intense peak at 527.6 eV is attributed to the oxygen in the metal oxide, the lower intensity peak at 529.5 eV is expected to be the oxygen in a surface hydroxyl, and the relatively small peak at 530.7 eV can be attributed to adsorbed molecular water and/or to the oxygen present in the organic contamination. The number of hydroxyl groups per unit area of TiO_2 nanoparticles was estimated using the reported method proposed by Dreiling[35] and then developed by Simmons and Beard.[36] Using the measured relative intensities of the O1s photoelectron signals from the hydroxyl and oxide, the hydroxyl concentration of the TiO_2 nanoparticles was calculated to be 4.08 hydroxyl/nm^2. This value is good agreement with the values those reported in the literature.[37–39]

XPS and FTIR results suggested that TiO_2 nanoparticles had significant amounts of hydroxyl groups on the surface. The initiators (MPTMS) were immobilized on the surface of the TiO_2 in one reaction step via ligand-exchanging reaction between the hydroxyl groups on the surface of TiO_2 and triethoxysilane

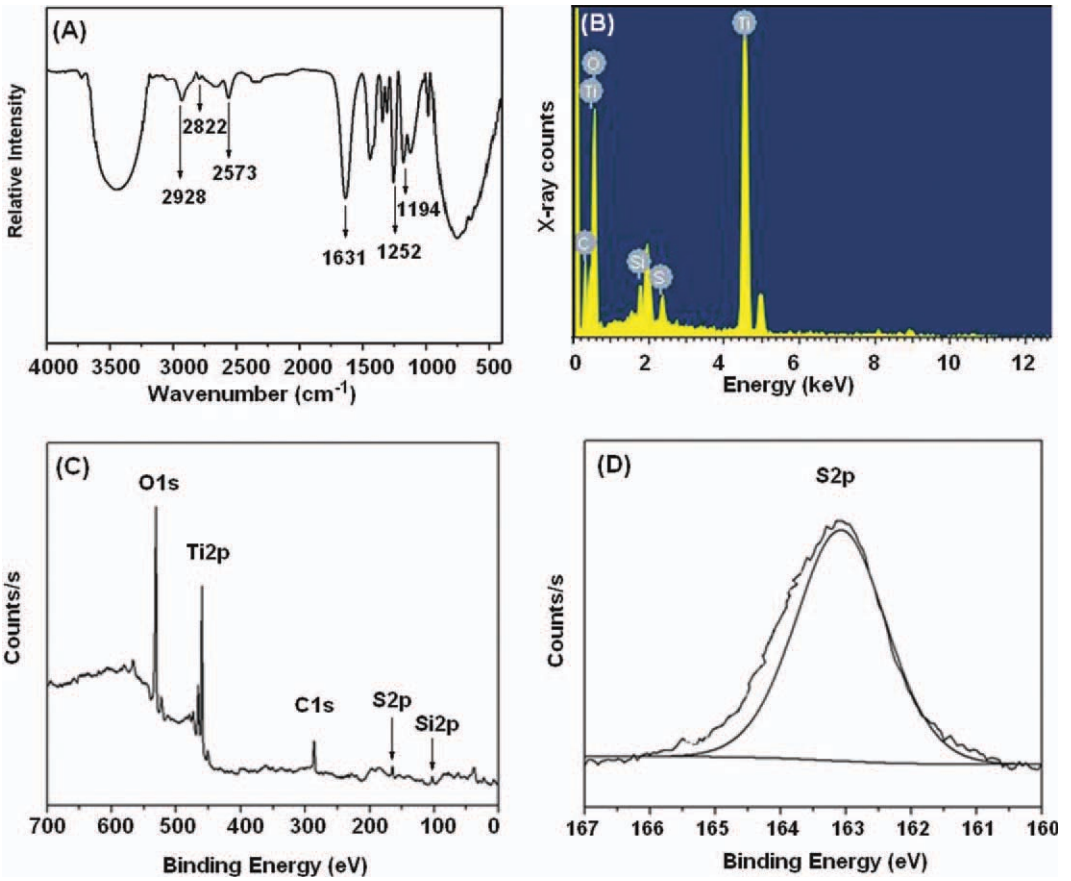

Figure 2. (A) FTIR spectrum, (B) EDX spectrum, (C) wide-scan spectrum, and (D) S2p core-level signals of TiO_2—SH nanoparticles. [Color figure can be viewed in the online issue, which is available at wileyonlinelibrary.com.]

groups of MPTMS to produce TiO_2—SH. The FTIR spectrum of TiO_2—SH shows the characteristic absorptions at 2822 and 2928 cm^{-1} due to the aliphatic C—H stretching of the coupling agent residues [Figure 2(A)]. Stretching vibration bands for Si—O—Si and Si—C bonds at 1194 and 1252 cm^{-1} are attributed to silane groups. The MPTMS functionalized TiO_2 nanoparticles gives a weak but visible absorption band at 2573 cm^{-1} is assigned to the S—H stretching band, which is not observed in the absorption spectrum of pristine TiO_2 nanoparticles, indicating the chemical anchoring of MPTMS onto TiO_2 nanoparticles. The EDX analysis of TiO_2—SH nanoparticles shows a small but detectable signal ascribed to the sulfur atoms on their surfaces [Figure 2(B)]. To verify the presence of thiol groups on TiO_2 nano-surfaces, the XPS experiment was carried out for TiO_2—SH [Figure 2(C)]. As expected, significant peaks for oxygen, titanium, carbon, sulfur, and silicon were observed. It is noteworthy that the characteristic S2p peak of the S—H bond is observed at 163.1 eV, which confirms the presence of active thiol groups on TiO_2 surfaces [Figure 2(D)].

The surface initiated grafting polymerization of HEMA from TiO_2 nanoparticles was carried out in the presence of TiO_2—SH and BL to afford PHEMA-*g*-TiO_2 nanocomposites. In the FTIR spectrum of PHEMA-*g*-TiO_2, the broad absorption band at 3022–3647 cm^{-1} is due to the O—H stretching and an increase in intensity at 2927 cm^{-1} is due to C—H stretching [Figure 3(A-i)]. A new absorption band which appears at 1724 cm^{-1} indicates the characteristic carbonyl (C=O) stretching band. The absorption bands at 1180–1225 cm^{-1} may originate from the stretching vibrations of —C—O— in the ester groups. The broad absorption bands at 500–800 cm^{-1} correspond to Ti—O—Ti stretching vibrations which appear in all the TiO_2 related samples, and the peak observed at 1634 cm^{-1} indicates the presence of physically adsorbed water in the TiO_2 samples.[24] The FTIR spectrum of the PHEMA cleaved from the PHEMA-*g*-TiO_2 nanocomposites [Figure 3(A-ii)] shows multiple bands at 3450 (O—H stretching) and 1728 cm^{-1} (—C=O stretching). The bands in the range of 2700–2950 cm^{-1} are attributed to C—H stretching of methyl (—CH_3) and methylene (—CH_2—) groups, and the band at 1450 cm^{-1} is ascribed to —C—H bending. These FTIR results suggest that the grafting polymerization of HEMA from TiO_2 nanoparticles surface via the TiO_2-SH/BL initiated process was successfully occurred.

Furthermore, the EDX scan of PHEMA-*g*-TiO_2 nanocomposites reveals the characteristic peaks of Ti, C, O, S, and Si as shown in the Figure 3(B). The XPS spectrum of PHEMA-*g*-TiO_2 nanocomposites is fully consistent with what is expected from a monolayer of PHEMA. After grafting of PHEMA, the C1s peak with high intensity slightly shifted to a higher binding energy (BE) [Figure 3(C)] than ungrafted TiO_2 nanoparticles [Figure 1(C)], indicating that the polymeric chains were directly grafted

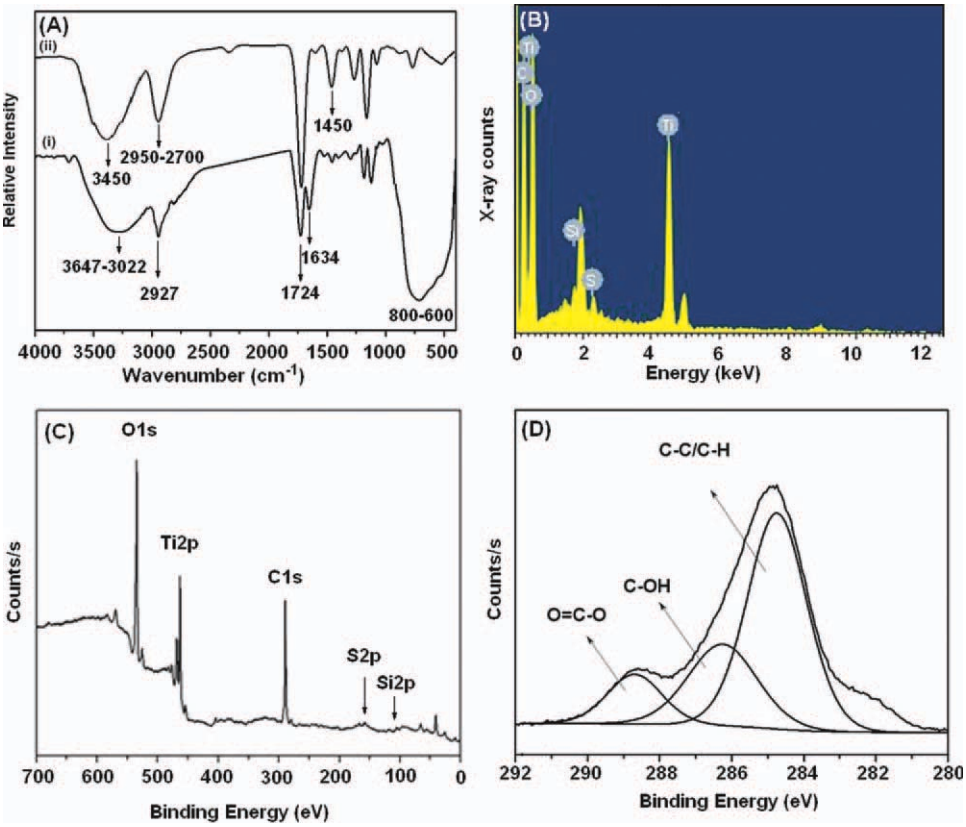

Figure 3. (A) FTIR spectra of (i) PHEMA-*g*-TiO_2 and (ii) the cleaved PHEMA (from PHEMA-*g*-TiO_2 nanocomposites); (B) EDX scan; (C) wide-scan spectrum, and (D) C1s core-level signals of PHEMA-*g*-TiO_2 nanocomposites. [Color figure can be viewed in the online issue, which is available at wileyonlinelibrary.com.]

from the surfaces of TiO_2 nanoparticles. The narrow scan C1s core-level spectra of PHEMA-*g*-TiO_2 show BE values of 284.6, 286.3, and 288.8 eV which are assigned to the C—H, C—OH, and O=C—O, respectively [Figure 3(D)].[20]

To analyze the structure and molecular weight of the grafted polymer, the grafted polymer chains were cleaved from PHEMA-*g*-TiO_2 nanocomposites using aqueous HCl. The ^{1}H-NMR spectrum of the cleaved PHEMA is shown in Figure 4(A). The peaks at 0.8–1.05 ppm (b) are mainly attributable to the protons of methyl groups of C—CH_3 in the polymer backbone and the broad peak at 2.02–2.11 ppm can be assigned to the hydroxyl proton (e). The peaks at 1.81, 3.81, and 4.04 ppm could be ascribed to the methylene protons of (a), (d), and (c), respectively, which are based on the backbone protons of the PHEMA. The peaks at 4.9 and 3.3 ppm can be attributed to the CH_3OH solvent peaks. The ^{1}H-NMR analysis further suggests that the synthesis of PHEMA-*g*-TiO_2 was successful. The number-average molecular weight (M_n) and molecular weight distribution (PDI) of the cleaved PHEMA was determined to be 15.900 g/mol and 1.34, respectively, as measured by the GPC analysis [Figure 4(B)].

To examine the composition effect on the thermal degradation of the PHEMA-*g*-TiO_2 nanocomposites, TGA analysis was performed for all the samples in the temperature range from 50 to 800°C (Figure 5). The pristine TiO_2 nanoparticles lost 2.1% of weight when it was heated from room temperature to 800°C, which may be due to the weight loss of the hydroxyl groups and adsorbed matters on TiO_2 nanoparticles [Figure 5(A)]. The modified TiO_2—SH lost 6.5% of weight at temperature 800°C as shown in Figure 5(B). The TGA curve of PHEMA-*g*-TiO_2 nanocomposites shows a major weight loss in the temperature range from 285 to 430°C which is possibly due to the presence of a significant amount of the combustible polymer [Figure 5(C)].

The char yards and decomposition temperature (T_d) (at 20% and 35% weight loss rate) of the cleaved PHEMA and PHEMA-*g*-TiO_2 nanocomposites are shown in Table I. In an attempt, it was observed that the PHEMA lost 20% of weight at the T_d of 281°C, on the contrary PHEMA-*g*-TiO_2 nanocomposites lost the same weight at T_d of 359°C. The char yields of the cleaved PHEMA and PHEMA-*g*-TiO_2 nanocomposites at 800°C are 0.9% and 50.6%, respectively. This enhancement in the char formation in the nanocomposites could be ascribed to the higher heat resistance imparted by the TiO_2.

The XRD patterns of the pristine TiO_2 nanoparticles, TiO_2-SH, PHEMA-*g*-TiO_2 and the cleaved PHEMA (from PHEMA-*g*-TiO_2 nanocomposites) in the 2θ range 5–80° are shown in Figure 6. Surface-initiated thiol-lactam polymerization can be considered to be an efficient way to realize the covalent connection of polymer chains with inorganic particles. However, changes in the

Applied Polymer SCIENCE

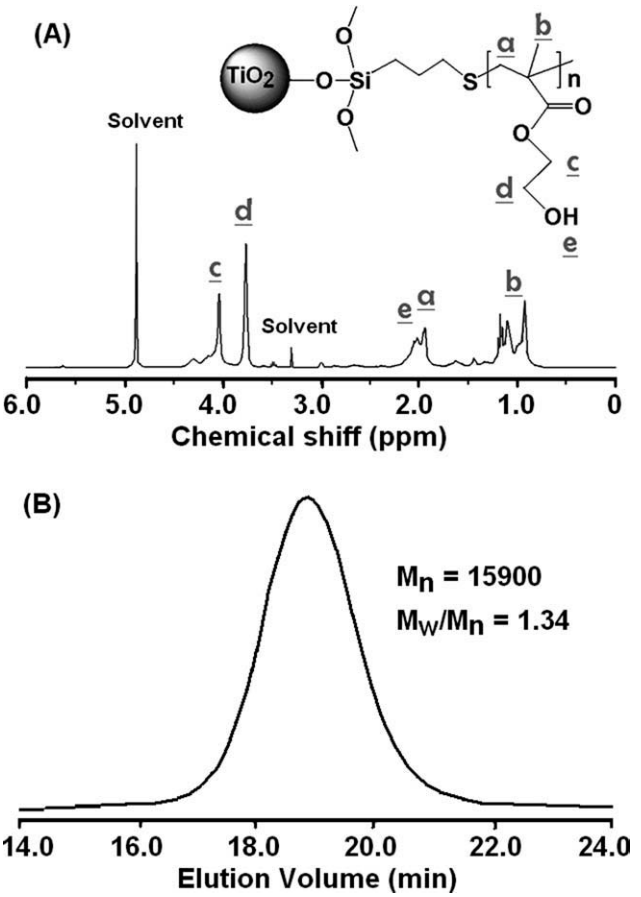

Figure 4. (A) ^{1}H-NMR spectrum and (B) the GPC trace of the cleaved PHEMA from PHEMA-*g*-TiO_2 nanocomposites.

bulk properties or original crystalline state as well as the intrinsic properties of the nanoparticles are not desirable. Thus, to ensure the selective reaction on the TiO_2 surfaces along with the maintenance of crystalline properties of TiO_2 is one of the most desired strategy. The pristine TiO_2 nanoparticles exhibited several sharp peaks centered at 2θ = 25.46, 37.89, 48.18, 54.10, 55.18, 62.77, 69.04, 70.28, and 76.47, which correspond to the (101), (112), (200), (105), (211), (204), (116), (220), and (215) reflections, respectively, suggesting the anatase form of TiO_2 nanoparticles [Figure 6(A)].[27] In the XRD scans, the main peaks of TiO_2—SH and PHEMA-*g*-TiO_2 nanocomposites are similar to those of TiO_2 nanoparticles. Upon surface modification of TiO_2 nanoparticles with PHEMA, a broad amorphous band with a 2θ value of 15.7° appeared, indicating the amorphous state of PHEMA. The presence of amorphous peaks is attributable to the molecular structures of the polymers. However, the surface modification did not show any significant effect on the crystallinity of TiO_2 nanoparticles. It indicates that the nanocomposites possess a more ordered orientation than the neat polymer owing to the inclusion of TiO_2 nanoparticles. In addition, XRD pattern of the cleaved PHEMA, from nanocomposites, shows broad peak in the region of 2θ = 10–20° which indicates its amorphous state [Figure 6(D)]. All these results suggest that the covalent attachment of PHEMA with TiO_2 nanoparticles does not affect the crystallinity of nanoparticles besides a well-ordered structure.

Table I. The Char Yards and T_d (at 20% and 35% Weight Loss Rate) of the Cleaved PHEMA and PHEMA-*g*-TiO_2 Nanocomposites

Samples	$T_d^{20\%}$ (°C)	$T_d^{35\%}$ (°C)	Char yard at 800°C (%)
Cleaved PHEMA	281	358	0.9
PHEMA-*g*-TiO_2	359	408	50.6

FE-SEM and TEM were used to investigate the morphology of TiO_2 nanoparticles before and after grafting PHEMA. The SEM images of pristine TiO_2 nanoparticles and PHEMA-*g*-TiO_2 nanocomposites are shown in Figure 7. When compared to pristine TiO_2 nanoparticles [Figure 7(A)], the images of

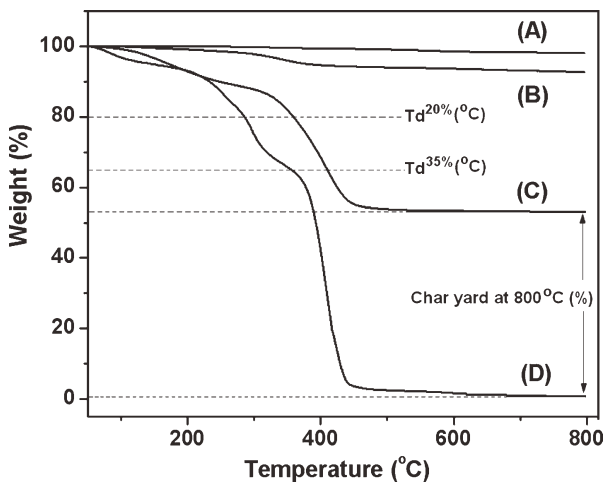

Figure 5. TGA scans of (A) pristine TiO_2 nanoparticles, (B) TiO_2—SH, (C) PHEMA-*g*-TiO_2 nanocomposites, and (D) the cleaved PHEMA (from PHEMA-*g*-TiO_2 nanocomposites).

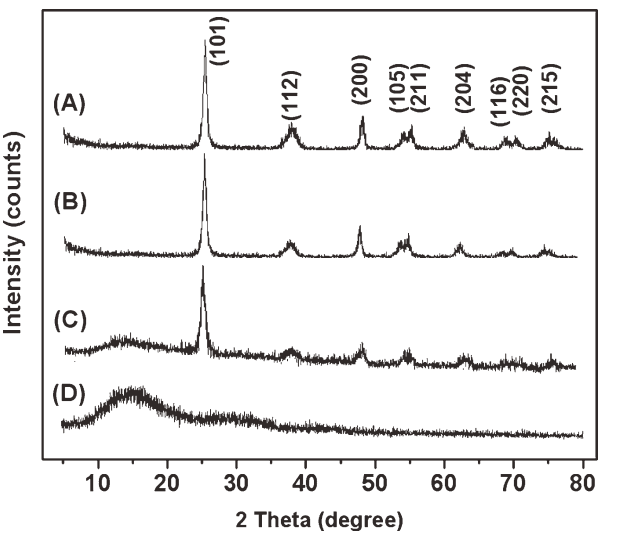

Figure 6. XRD patterns of (A) TiO_2 nanoparticles, (B) TiO_2—SH, (C) PHEMA-*g*-TiO_2, and (D) the cleaved PHEMA (from PHEMA-*g*-TiO_2 nanocomposites).

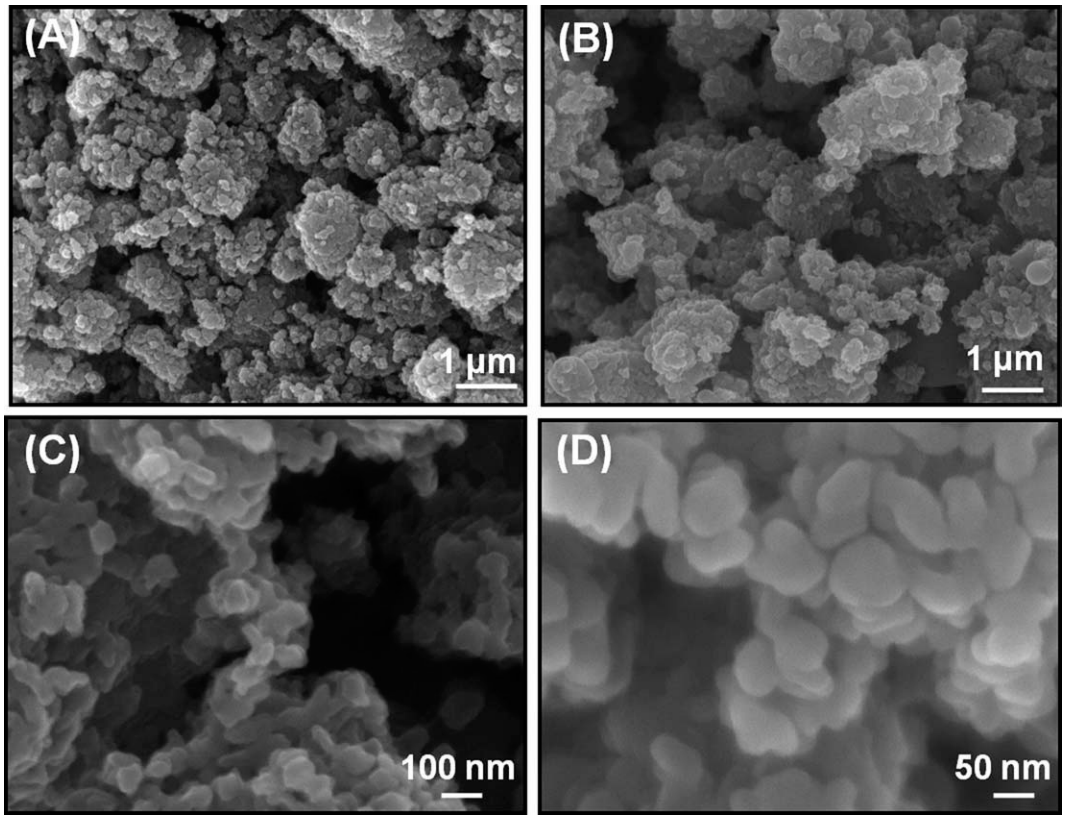

Figure 7. SEM images of (A) pristine TiO_2 nanoparticles, and (B, C, and D) PHEMA-*g*-TiO_2 nanocomposites at different magnifications.

nanocomposites [Figure 7(B, D)] demonstrate relatively spherical shape having the polymer layer, and it is observed that TiO_2 nanoparticles are embedded in the polymer beads.

The TEM images of pristine TiO_2 nanoparticles and PHEMA-*g*-TiO_2 nanocomposites are shown in Figure 8. The pristine TiO_2 nanoparticles shows aggregation of particles [Figure 8(A, B)] and the single electron diffraction pattern [inset Figure 8(A)] consisting of rings, which indicates a good crystal structure of the nanoparticle. In contrast, the PHEMA-*g*-TiO_2 nanocomposites are seen well dispersed which might be due to the steric hindrance exerted by the grafted PHEMA [Figure 8(C, D)]. These results suggest that the dispersibility of TiO_2 nanoparticles is strongly influenced by the surface functionalization of nanoparticles.

For different applications of nanoparticles, a key parameter is their well dispersibility in either various solvents or polymeric matrices. Upon modification of TiO_2 nanoparticles via covalent immobilization of PHEMA, it was expected to prevent aggregation of the nanoparticles and improved their dispersion stability in solvents or polymer matrices. The photographs of dispersion experiments of pristine TiO_2 nanoparticles and PHEMA-*g*-TiO_2 nanocomposites in toluene are shown in Figure 9. The pristine TiO_2 nanoparticles were found to be completely settled down within a few minutes of being dispersed, whereas the PHEMA-*g*-TiO_2 demonstrated improved dispersibility and remained stable for prolonged period. This remarkable difference in the dispersibility between pristine TiO_2 nanoparticles and PHEMA-*g*-TiO_2 nanocomposites could be explained in such a way that the PHEMA chain might act as a steric stabilizing layer to prevent agglomeration which dramatically increased the colloidal stability in organic solvent. This result suggests that the agglomeration propensity of TiO_2 nanoparticles was remarkably reduced upon covalent grafting of PHEMA. In addition, to obtain information on the size and size distribution of PHEMA-*g*-TiO_2 nanocomposites the DLS measurement was undertaken as shown in Figure 9(C). From the DLS measurements, the average size of PHEMA-*g*-TiO_2 nanocomposites in methanol was estimated to be 160 ± 13 nm, suggesting their potential for utility in biomedical applications.

CONCLUSIONS

In this work, a facile method to synthesize covalently immobilize PHEMA onto TiO_2 nanoparticles using the grafting from approach has been demonstrated. At first, TiO_2 nanoparticles were treated with MPTMS to afford thiol functional surface (TiO_2—SH). The surface initiated polymerization of HEMA with the aid of TiO_2—SH and BL afforded PHEMA-*g*-TiO_2 nanocomposites. The surface initiated radical polymerization was studied by FTIR, ^{1}H-NMR, XPS, XRD, TGA, TEM, and SEM analyses. The FTIR data suggested that a covalent bond was formed between TiO_2 nanoparticles and PHEMA in the nanocomposites. The molecular weight and PDI of the cleaved PHEMA from PHEMA-*g*-TiO_2 nanocomposites were measured to be 15,900 and 1.34, respectively. It was observed that surface

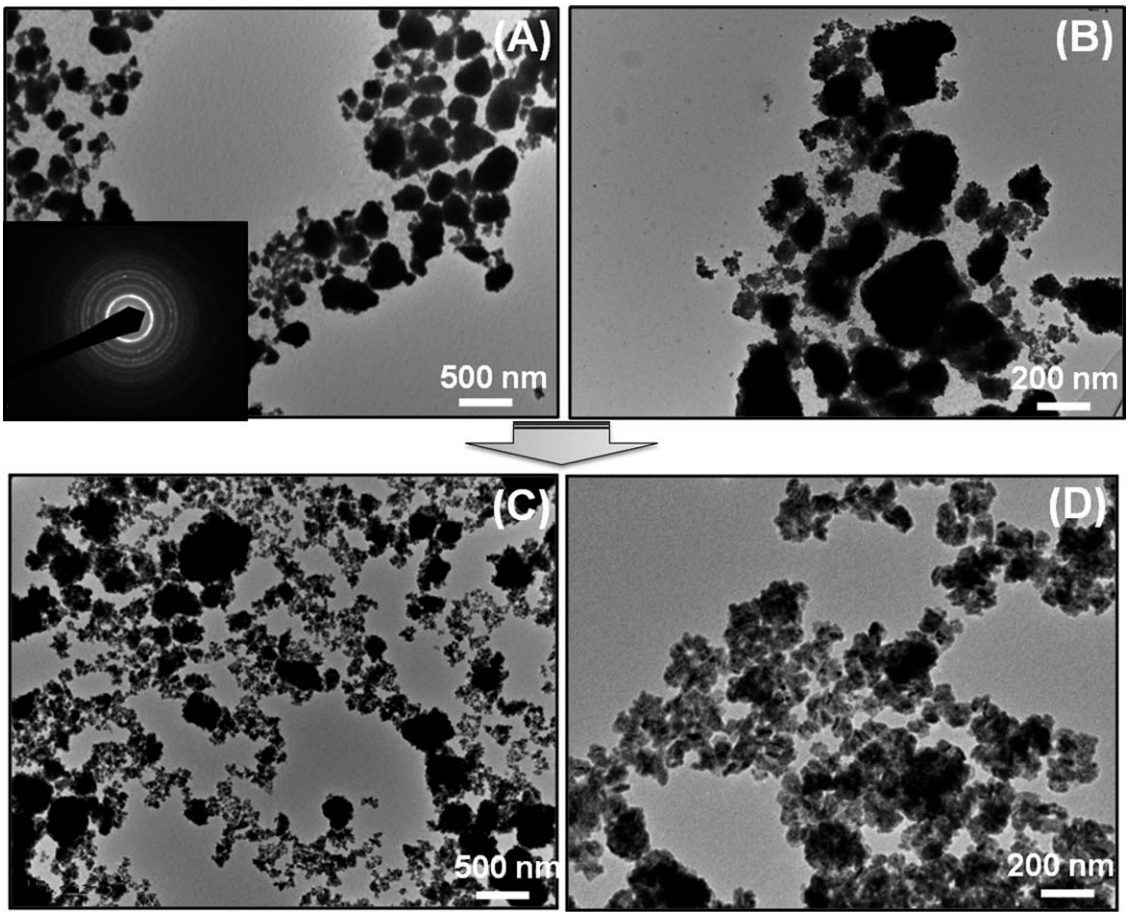

Figure 8. TEM pictures of (A) pristine TiO_2 nanoparticles and (C) PHEMA-*g*-TiO_2 nanocomposites; pictures (B) and (D) are different magnifications of (A) and (C), respectively.

functionalization using the grafting from strategy did not alter the physical structure of TiO_2 nanoparticles as suggested by the XRD analysis. At the rate of 20% weight loss, the decomposition temperature of cleaved PHEMA was found to be 281°C, in contrast, at the similar condition the decomposition temperature of PHEMA-*g*-TiO_2 nanocomposites was observed to be 359°C as determined using TGA scan. The char yields of the cleaved PHEMA and PHEMA-*g*-TiO_2 nanocomposites at 800°C were calculated to be 0.9% and 50.6%, respectively. The TEM results suggest that the agglomeration tendency of TiO_2 nanoparticles was significantly reduced. The grafting of PHEMA significantly increased the colloidal stability of TiO_2 nanoparticles in organic solvent. The hydrodynamic diameter of PHEMA-*g*-TiO_2 nanocomposites in methanol was measured to be 160 ± 13 nm.

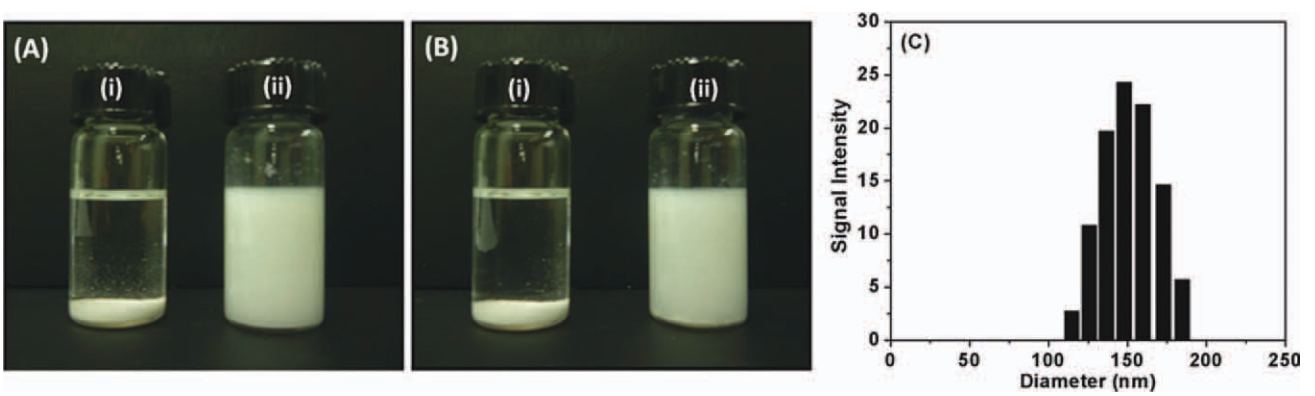

Figure 9. Photographs of (i) pristine TiO_2 nanoparticles and (ii) PHEMA-*g*-TiO_2 nanocomposites dispersion in toluene after (A) 15 min, and (B) 12 h; (C) the hydrodynamic diameters of PHEMA-*g*-TiO_2 nanocomposites. [Color figure can be viewed in the online issue, which is available at wileyonlinelibrary.com.]

ACKNOWLEDGMENTS

This work was financially supported by the Joint Program of Cooperation in Science and Technology through NRF grant funded by the MEST (No. 2011-0025680).

REFERENCES

1. Hao, R.; Xing, R.; Xu, Z.; Hou, Y.; Gao, S.; Sun, S. *Adv. Mater.* **2010,** *22*, 2729.
2. Daniel, M. C.; Astruc, D. *Chem. Rev.* **2004,** *104*, 293.
3. Ramakrishna, S.; Mayer, J.; Wintermantel, E.; Leong, K. W. *Compos. Sci. Tech.* **2001,** *61*, 1189.
4. Rezwan, K.; Chen, Q. Z.; Blaker, J. J.; Boccaccini, A. R. *Biomaterials* **2006,** *27*, 3413.
5. Armentano, I.; Dottori, M.; Fortunati, E.; Mattioli, S.; Kenny, J. M. *Polym. Degrad. Stab.* **2010,** *95*, 2126.
6. Webster, T. J.; Siegel, R. W.; Bizios, R. *Biomaterials* **1999,** *20*, 1221.
7. Savaiano, J. K.; Webster, T. J. *Biomaterials* **2004,** *25*, 1205.
8. Gerhardt, L. C.; Jell G. M. *R.; Boccaccini, A. R. J. Mater. Sci.: Mater. Med.* **2007,** *18*, 1287.
9. Fray, M. E.; Boccaccini, A. R. *Mater. Lett.* **2005,** *59*, 2300.
10. Kong, H. Y.; Song, J. Y.; Jang, J. S. *Environ. Sci. Technol.* **2010,** *44*, 5672.
11. Zheng, M. P.; Jin, Y. P.; Jin, G. L.; Gu, M. Y. *J. Mater. Sci. Lett.* **2000,** *19*, 433.
12. Roether, J. A.; Boccaccini, A. R.; Hench, L. L.; Maquet, V.; Gautier, S.; Jerome, R. *Biomaterials* **2002,** *23*, 3871.
13. Yoshikawa, C.; Goto, A.; Tsujii, Y.; Ishizuka, N.; Nakanishi, K.; Fukuda, T. J. *Polym. Sci. Part A: Polym. Chem.* **2007,** *45*, 4795.
14. Mei, Y.; Wu, T.; Xu, C.; Langenbach, K. J.; Elliott, J. T.; Vogt, B. D. *Langmuir* **2005,** *21*, 12309.
15. Brahim, S.; Narinesingh, D.; Elie, A. G. *Biomacromolecules* **2003,** *4*, 497.
16. Li, D.; Chen, H.; Wang, S.; Wua, Z.; Brash, J. L. *Acta Biomater.* **2011,** *7*, 9541.
17. Young, C. D.; Wu, J. R.; Tsou, T. L. *Biomaterials* **1998,** *19*, 1745.
18. Zhang, F.; Shi, Z. L.; Chua, P. H.; Kang, E. T.; Neoh, K. G. *Ind. Eng. Chem. Res.* **2007,** *46*, 9077.
19. Stengl, V.; Houskova, V.; Bakardjieva, S.; Murafa, N.; Havlın, V. *J. Phys. Chem. C* **2008,** *112*, 19979.
20. Prashantha, K.; Rashmi, B. J.; Venkatesha, T. V.; Lee, J. H. *Spec. Chem. Acta Part A: Mol. Biomol. Spectrosc.* **2006,** *65*, 340.
21. Li, C.; Zheng, Y. F.; Lou, X. *J. Mater. Sci.: Mater. Med.* **2009,** *20*, 2215.
22. Gorbovyi, P.; Uklein, A.; Tieng, S.; Brinza, O.; Traore, M.; Chhor, K.; Museur, L.; Kanaev, A. *Nanoscale* **2011,** *3*, 1807.
23. Bach, L. G.; Islam, M. R.; Jeong, Y. T.; Gal, Y. S.; Lim, K. T. *Appl. Surf. Sci.* **2012,** *258*, 2816.
24. Wang, W.; Cao, H.; Zhu, G.; Wang, P. *J. Polym. Sci. Part A: Polym. Chem.* **2010,** *48*, 1782.
25. Ngo, V. G.; Bressy, C.; Leroux, C.; Margaillan, A. *Polymer* **2009,** *50*, 3095.
26. Matsuno, R.; Otsuka, H.; Takahara, A. *Soft Matter* **2006,** *2*, 415.
27. Park, J. T.; Koh, J. H.; Koh, J. K.; Kim, J. H. *Appl. Surf. Sci.* **2009,** *255*, 3739.
28. Barbey, R.; Lavanant, L.; Paripovic, D.; Schuwer, N.; Sugnaux, C.; Tugulu, S.; Klok, H. A. *Chem. Rev.* **2009,** *109*, 5437.
29. Park, J. T.; Seo, J. A.; Ahn, S. H.; Kim, J. H.; Kang, S. W. *J. Ind. Eng. Chem.* **2010,** *16*, 517.
30. Hojjati, B.; Charpentier, P. A. *J. Polym. Sci. Part A: Polym. Chem.* **2008,** *46*, 3926.
31. Xiong, L.; Liang, H.; Wang, L.; Chen, L. *J. Polym. Res.* **2011,** *18*, 1017.
32. Park, J. T.; Koh, J. H.; Seo, J. A.; Kim, J. H. *J. Mater. Chem.* **2011,** *21*, 17872.
33. Mesnage, A.; Magied, M. A.; Simon, P.; Boime, N. H.; Jegou, P.; Deniau, G.; Palacin, S. *J. Mater. Sci.* **2011,** *46*, 6332.
34. Hwang, H. S.; Bae, J. H.; Kim, H. G.; Lim, K. T. *Eur. Polym. J.* **2010,** *46*, 1654.
35. Rashid, M. H.; Bae, J. H.; Park, C.; Lim, K. T. *Mol. Cryst. Liq. Cryst.* **2010,** *532*, 514.
36. Bach, L. G.; Islam, M. R.; Kim, J. T.; Seo, S. Y.; Lim, K. T. *Appl. Surf. Sci.* **2012,** *258*, 2959.
37. Dreiling, M. *J. Surf. Sci.* **1978,** *71*, 231.
38. Simmons, G. W.; Beardt, B. C. *J. Phys. Chem.* **1987,** *91*, 1143.
39. Erdem, B.; Hunsicker, R. A.; Simmons, G. W.; Sudol, E. D.; Dimonie, V. L.; El-Aasser, M. S. *Langmuir* **2001,** *17*, 2664.